Atomic Oxygen Testing with Thermal Atom Systems: A Critical Evaluation

Steven L. Koontz,* Keith Albyn,† and Lubert J. Leger‡
NASA Johnson Space Center, Houston, Texas 77058

The use of thermal atom (kinetic energy near 0.04 eV) test methods as a materials selection and screening technique for low-Earth-orbit (LEO) spacecraft is critically evaluated in this paper. The physics and chemistry of the thermal atom environments are shown to produce specific mass loss rates (mg cm^{-2} min^{-1}) and reaction efficiencies (*Re*) radically different from those produced in the LEO environment. A response surface study shows that specific mass loss rates change rapidly with plasma-asher parameters and seldom agree with flight data. FEP Teflon is shown to react by a different mechanism than Kapton, polyethylene, or graphite. The *Re* (*Re* = volume of material removed per oxygen atom) of Kapton, polyethylene, Mylar, Tedlar, FEP Teflon, and graphite measured in a flowing afterglow apparatus are 10^{-3} to 10^{-4} those measured with high-energy atoms (kinetic energy 1.5 eV or greater) in beam systems or in LEO. The effect of sample temperature and atom impact energy on *Re* is discussed. A simple kinetic model describing the reaction of atomic oxygen with polymer surfaces is developed. Guidelines and recommendations for thermal atom testing and interpretation of test results are presented.

Introduction

MATERIALS degradation resulting from atomic oxygen attack is an important long life issue for spacecraft operating in the low-Earth-orbit (LEO) environment. The cost and limited availability of materials test time in flight or in high-quality LEO environment simulators have generated considerable interest in the use of thermal energy (kinetic energy on the order of 0.04 eV; O^3P electronic ground state) oxygen atoms for materials testing. Thermal atom methods include oxygen plasma ashing, low-pressure flowing discharges, and thermal energy beams.

In this paper a critical evaluation of the various thermal atom test methods is presented. The important differences between the thermal atom test environments and the LEO environment are reviewed as are the ways in which various environmental factors influence materials-reactivity measurements. Finally, thermal atom materials-reactivity measurements are compared with measurements made in LEO or in the high-quality LEO simulation at Los Alamos National Laboratory (LANL). The dependence of materials reactivity on atom translational energy, sample temperature, and other environmental factors is discussed. The reactivities of organic materials and graphites are the primary focus of this paper. Metals, ceramics, and optical coatings are not discussed.

LEO Environment

Spacecraft operating at altitudes between 200 and 900 km are operating in LEO, where the residual atmosphere is composed predominantly of oxygen atoms and nitrogen molecules.[1,2] The molecular oxygen density is less than one-tenth the atomic oxygen density over this altitude range.[1,2] Spacecraft orbiting at these altitudes travel at velocities of 8–12 km/s (depending on orbital eccentricity), so that ambient oxygen atoms strike ram-oriented spacecraft surfaces with translational energies of 5–8 eV. The atom flux depends on altitude, solar activity, orbital inclination, and time of day,[1,2] with $10^{14}-10^{15}$ atoms cm^{-2} s^{-1} being a nominal range of values for Space Station Freedom. The effects of the oxygen atom ram flux on about 300 different materials have been investigated in three Space Shuttle flight experiments and one satellite recovery and are summarized in Table 1. Detailed treatments of the flight data are found in Refs. 3–23. Impact on spacecraft design is discussed in Refs. 24–26. It has been well established that oxidation reactions are the mechanistic basis for materials degradation by atomic oxygen in LEO.[16] No significant contributions from ablation or sputtering have been demonstrated to date.

In addition to oxygen atoms, surfaces in the LEO environment encounter low-energy charged particles (ionospheric plasma), some high-energy charged particles (from radiation belts and cosmic rays), solar ultraviolet (UV), and vacuum ultraviolet (VUV). Synergism between oxygen and other environmental factors should influence the reaction efficiencies of materials in some circumstances. A VUV atomic oxygen synergism in the degradation of fluorocarbon materials has recently been demonstrated in the laboratory.[27]

The thermal atom environments reviewed in this work are compared with the LEO environment in a general way in Table 2.[28,29] As can be seen in Table 2, thermal atom test environments differ significantly from the LEO environment in several important respects. The differences between the LEO environment and the various thermal atom environments naturally reduce the credibility of any thermal atom test system.

Table 1 Materials reactivity data in LEO and LANL beam

Material	Reaction efficiency *Re*, cm^3/atom LEO[3-23]	LANL[24,60]
Kapton	3.0×10^{-24}	2.7×10^{-24}
Polyethylene	3.7×10^{-24}	2.8×10^{-24}
FEP Teflon	$<0.05\times10^{-24}$	7.7×10^{-25}
Mylar	3.4×10^{-24}	—
Tedlar	3.2×10^{-24}	—
Graphite (various)	$0.9-1.7\times10^{-24}$	10^{-24}
Polybenzimidazole	1.5×10^{-24}	—
Polysulfone	2.4×10^{-24}	—
Siloxane-imide block copolymers (25%/75%)	0.3×10^{-24}	—
Epoxy	1.7×10^{-24}	—

Received Oct. 10, 1989; revision received March 16, 1990; accepted for publication April 10, 1990.

*AST Materials. Member AIAA.
†AST Materials.
‡Materials Branch Chief. Associate Fellow AIAA.

Table 2 Comparison of environments

Environment	Oxygen atom flux,[a] energy	O_2 molecule flux,[a] energy	Electron density, energy	VUV flux,[a] wavelength
LEO	10^{15}, 5 eV	10^{13}, 10 eV	10^5–10^6 cm^{-3}, 0.1 eV	~4 × 10^{11}, 121.6 nm
Plasma asher	10^{19}–10^{20}, 0.04–0.06 eV	10^{21}, 0.04–0.06 eV	10^9–10^{12} cm^{-3}, 1–10 eV	10^{12}–10^{14}, 130 nm
Flowing afterglow	10^{18}–10^{19}, 0.04 eV	10^{21}, 0.04 eV	$<10^8$ cm^{-3}, 0.04 eV	0

[a]Flux units are particles (cm^{-2} s^{-1}).

A test system producing a perfect reproduction of the LEO environment requires less validation than one which produces a wide range of extraneous environmental factors.

An important fundamental difference between the LEO or laboratory atom beam environments and the thermal atom environments discussed below involves the concept of thermodynamic equilibrium. In LEO, the reacting surface (about 0.04 eV thermal energy or about 300 K) and the incoming atomic oxygen ram flux (5 eV translational energy, equivalent to about 60,000 K) are not in thermodynamic equilibrium. We have a hot atom beam reacting with a cold surface and the influence of surface temperature on reaction rate can be studied independent of atom impact energy. In thermal atom systems operating at pressures greater than 0.1 Torr, the sample and the gas above it are close to thermodynamic equilibrium simply because the mean free path is much smaller than the dimension of any heated surface, and the steady-state temperature gradients near the heated surface are small. As a result, surface temperature and atom-surface collision energy are coupled in thermal atom systems, and the variation in atom impact energy that can be achieved without pyrolysis of most polymers is small (300–800 K).

Radio Frequency Plasma-Asher Environment

Oxygen plasmas have been used for photoresist etching and multilayer lithography for many years now and have been the subject of a recent critical review.[30] The radio frequency (RF) plasma asher can be operated over a fairly wide range of pressures and RF powers, producing a wide range of environments. When operating with pure oxygen as the working gas, the atomic oxygen yield can vary from 1 to 60% depending on a number of operating variables. Unfortunately, direct measurement of atomic oxygen densities is not a feature available in off-the-shelf plasma asher or plasma-etching systems. Similarly, charged-particle density, density of excited-state neutrals, temperature, and ultraviolet (UV and VUV) flux and spectra can vary over fairly wide ranges.[30-33] Asher environments share one common factor, however. The sample material is always exposed directly to a plasma and an RF field, unless a Faraday cage is used to enclose the sample material.[34] The RF field can heat conducting samples, or samples containing conducting components, by induction. Charged-particle bombardment of the sample can dramatically change the measured reactivity[38-40] and is a common technique for controlling morphology and reactivity in the fabrication of semiconductor devices.[38-40]

Four important differences between the LEO environment and the thermal atom environments are apparent (see Table 2): 1) the kinetic energy of the oxygen atoms; 2) the very large difference in molecular oxygen flux; 3) the high flux of UV and VUV photons; and 4) the high flux of charged particles and excited-state neutrals.

For a dissociation yield of 2% at a total pressure of 2 Torr, the oxygen molecule flux on any surface in the plasma is 7×10^{20} molecules cm^{-2} s^{-1} while the atom flux is only 4×10^{19}. By themselves, the oxygen molecules are relatively inert (none of the materials examined in this study are air sensitive), but they can react with surface alkyl radicals created by oxygen atom attack. The formation of peroxy radicals from alkyl radicals and molecular oxygen in the gas phase[41] is well known. Polymer surfaces exposed in asher and afterglow environments contain more surface oxygen than those exposed to the LEO environment.[42]

Vacuum ultraviolet radiation deserves special mention because low-pressure discharges in oxygen are an efficient means of generating the 130-nm (9.4 eV) resonance line of atomic oxygen. The flux of solar radiation with wavelengths between 150 and 100 nm is only 0.75 μW per cm^2 in LEO.[43] In discharge lamps, and plasma ashers, the flux at the oxygen line can be thousands of times higher providing more opportunity for photochemistry with these high-energy, bond-breaking photons.[44,45]

Flowing Afterglow Environment

The flowing afterglow environment is much easier to define than the plasma-asher environment. In the flowing afterglow method, a gas containing oxygen flows through a microwave or RF discharge region where oxygen atoms are produced.[46,47] The gas then flows out of the discharge region and cools to near room temperature before contacting the surface of the test material. The flowing afterglow has a long and venerable history as a device for studying the kinetics of ground-state (O^3P) oxygen atom reactions in the gas phase[46-49] but has seen only limited use in the study of surface reactions.[50-55] The total pressure of the gas is usually between 0.1 and 2 Torr. Pure oxygen or oxygen diluted in an inert gas such as argon or helium may be used.[46-48] Accurate atomic oxygen concentration measurements can be accomplished by one of several methods.[29,46] The flowing afterglow environment used in this work consists of a gas at or near room temperature containing argon atoms, oxygen atoms, and oxygen molecules, predominantly in the electronic ground state.[29,46,47] The concentration of excited-state neutrals, ions, and electrons is negligible,[29,46,47] and it is easy to configure the test specimen so that no electromagnetic radiation from the discharge zone reaches the sample.

If the concentration of oxygen atoms and the temperature in the gas near the sample surface can be measured or estimated, the atom flux and kinetic energy at the surface can be calculated from classical kinetic theory.[56,57] The surface flux is simply the atom concentration near the surface multiplied by one-fourth the gas kinetic speed ($F=[O]v/4$), and the average atom kinetic energy can be calculated directly from the Boltzman equation ($E=3kT/2$).

Atoms reaching the surface are lost as a result of reaction with the substrate or recombination to form molecular oxygen or ozone (O_3). The atom concentration near a reactive surface depends on the relative rates of transport to, and atom loss at, the surface, as well as losses in the gas phase and on other surfaces in the system.[46,47,58] An analysis of the transport/reaction process is a vital part of test system design and an important aid in understanding test data. The sidearm sample configuration used in the afterglow apparatus described in the following is amenable to exact transport analysis resulting in accurate estimates of atom flux at the sample surface in most cases.[59,60]

The major differences between the asher and the afterglow rest in the flux of excited species, charged particles, and UV photons at the sample surface, which is much smaller for the afterglow than the asher.[29,32,46] In the afterglow described in this paper, temperature can be set independently of other parameters (a capability not always available in commerical

plasma ashers), allowing the activation energy of the atomic oxygen reaction to be determined.

Experimental

An LFE Corporation LTA-302 low-temperature, inductively coupled plasma asher was used in this study. Experimental configurations and methods employing the asher have been reported previously[60] and are briefly summarized here. The asher chamber and sample-holder configuration are shown in Fig. 1. The asher operates at 13.56 MHz. Test specimens were placed in a Pyrex glass sample holder positioned horizontally on the long axis of the asher chamber. The working gas used in the asher was aviators breathing oxygen (MIL-0-27210 E). A cylindrical Faraday cage made of perforated aluminum positioned the sample holder on the chamber axis as shown in Fig. 1 for measurements without direct sample-plasma contact. Specific mass loss rates (mass loss rate per unit exposed area) were determined using several different asher operating conditions as part of a simple response surface study.

Relative measurements of VUV flux at the sample-holder position were made using a VUV phosphor described by Watanabe.[61] The visible fluorescence produced by VUV radiation incident on the phosphor was observed visually through the asher chamber doors.

The flowing afterglow apparatus is shown in Fig. 2 and is similar to the afterglow systems described in Refs. 27 and 60. A brief description of the afterglow system and methods used in this study is given in the following.

An Evenson-type[29,46,47] cavity was used to generate a microwave discharge in a low-pressure (about 2 Torr) flowing gas. After passing through the discharge cavity, the gas flows past a sidearm sample-holder assembly as previously described.[27,60] The sidearm sample holders were Pyrex tubes, 3 cm long, 1.42 cm i.d., and 1.90 cm o.d., with the tube axis-oriented perpendicular to the direction of gas flow. The thin-film sample disks were placed over the ends of the sidearm tubes so that 1.59 cm^2 of sample surface was exposed to the oxygen atom flux; the remainder of the sample was protected by the end of the sidearm tube. The samples were held in position by 1.90-cm-diam black anodized aluminum sample-holder plugs. Modified Cajon tubing unions maintained vacuum seal and held the sample-holder plug against the end of the sidearm tube. The square HOPG (highly oriented polycrystalline graphite) sample was merely allowed to rest flat on the end of a sample-holder plug. Sample temperature was varied using cartridge-type resistance heaters inserted into wells in the sample-holder plugs. Temperature was measured using type K thermocouples also inserted in the plugs. By varying the temperature of the sample-holder plugs, the activation energy of the atomic oxygen reaction could be determined.

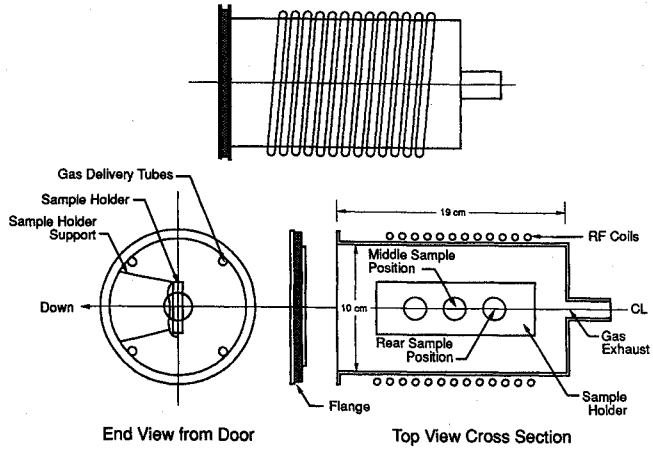

Fig. 1 Plasma asher apparatus configuration.

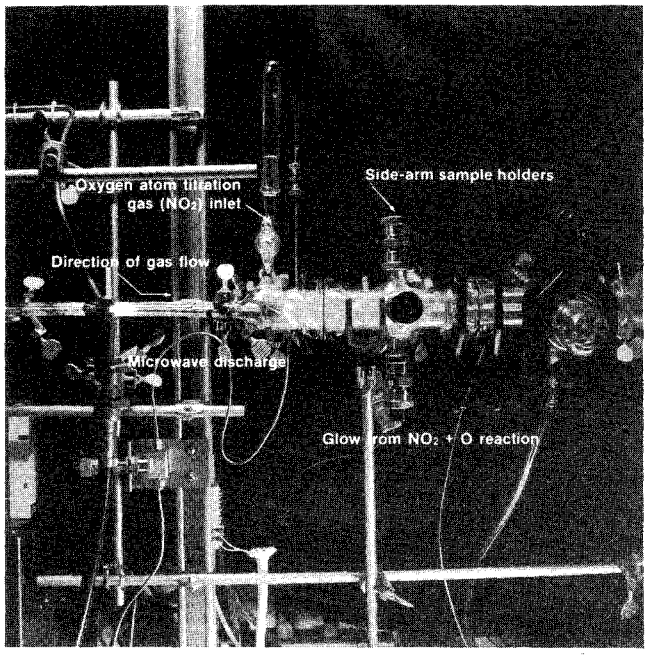

Fig. 2 Flowing afterglow apparatus.

Two working gases were used in the flowing afterglow apparatus: 1) aviators breathing oxygen (MIL-0-27210 E), and 2) 10% oxygen in argon (>99.995% pure). In some cases water vapor was added to the working gas stream to boost oxygen atom yield and examine the effects of water vapor in the working gas stream.

Afterglow oxygen atom concentrations were measured by chemiluminescent titration with NO_2[29,46] and with catalytic recombination probes prepared by coating copper-constantan thermocouples with molten silver.[29] Atomic oxygen concentration profiles were determined by taking recombination probe readings at several positions in the sidearm and at the titration point. Concentration profile data were combined with a reaction-transport model of the sidearm to yield atom concentrations near the sample surface.[59]

Kapton HN, FEP Teflon, polyethylene, Tedlar, and Mylar samples were all cut from sheets of 0.005-cm film. The Kapton, FEP Teflon, polyethylene, pyrolytic graphite, and HOPG were obtained from NASA's Lewis Research Center (LeRC) as part of the atomic oxygen effects test program (oxygen effects round-robin). Tedlar and Mylar film samples were obtained from E. I. du Pont de Nemours & Co., Inc. Perdeuteropolyethylene was obtained from Icon Servies, Inc., as a neat powder and was melt cast under nitrogen by Afton Plastics Molding Co. (care was taken to prevent surface contamination by silicones or fluorocarbons) to produce a 0.01-cm-thick film. All samples except the HOPG were cleaned by brief rinsing with optical grade solvent, a mixture of 1,1,1, trichloroethylene (75%) and ethanol (25%) from Analytical Research Laboratories, Monrovia, California. The same sample preparation procedure was used for Johnson Space Center (JSC) flight samples exposed during STS-8 and samples prepared for test in the LANL high-energy beam system. After air drying, the samples were stored in a dessicator at least 48 h before use (vacuum baking showed little effect on results in this study). Clean surfaces of HOPG were prepared by applying adhesive tape to the basal plane of the crystal and pealing of the top layer leaving a fresh, clean surface. The HOPG samples were squares, about 1 cm on an edge and less than 0.2 cm thick.

Samples were weighed, in air, on a Mettler Model H20T laboratory balance. Atomic oxygen reactivities were determined by removing the samples from the asher or afterglow

Table 3 Materials reactivity data, plasma-asher environments

Pressure, Torr	RF, W	Mass loss rates, mg min^{-1} cm^{-2} × 10^2 Kapton	Polyethylene	FEP Teflon	HOPG graphite
2	100	1.6±0.3	5.3±0.2	0.27±0.005	0.59±0.006
2	50	0.06±0.01	0.52±0.2	0.18±0.04	——
0.4	50	0.80±0.2	3.2±0.5	0.49±0.06	——
0.1	100	0.71±0.2	3.6±0.5	1.1±0.09	0.24±0.06
0.1	10	0.12±0.01	0.45±0.02	0.26±0.02	——

Table 4 Materials reactivity data, plasma-asher, Faraday-cage environments

Pressure, Torr	RF, W	Mass loss rates, mg min^{-1} cm^{-2} × 10^2 Kapton	Polyethylene	FEP Teflon	HOPG graphite
2	100	1.4±0.4	2.5±0.8	0.04±0.01	——
1	100	1.1±0.2	——	0.09±0.03	——
0.1	100	0.5±0.03	1.6±0.2	0.2±0.02	——

Table 5 Mass loss rates relative to Kapton, no Faraday cage

Pressure, Torr	RF, W	Specific mass loss rate divided by Kapton rate Kapton	Polyethylene	FEP Teflon	HOPG graphite
2	100	1.0	3.4	0.17	0.12
2	50	1.0	8.5	3.0	——
0.4	50	1.0	4.0	0.6	——
0.1	100	1.0	5.1	1.6	0.09
0.1	10	1.0	3.6	2.1	——

periodically for weighing followed by a simple linear-regression analysis to obtain the specific mass loss rate. For both the asher and the afterglow, the specific mass loss rate was used as the measure of reactivity with atomic oxygen. In the afterglow, reaction efficiencies (*Re* in cm^3/atom) were calculated from specific mass loss rate and atom flux at the sample surface.

Results: Plasma Asher

Atomic oxygen densities could not be measured or reasonably estimated in the asher, so that oxygen atom surface fluxes and reaction efficiencies, *Re*, could not be calculated. Specific mass loss rates were determined using several combinations of RF power and oxygen pressure to produce a response surface study. The specific mass loss rates (mg min^{-1} cm^{-2}) are shown for each asher operating condition in Table 3 (no Faraday cage) and Table 4 (Faraday cage). In Tables 5 (no Faraday cage) and 6 (Faraday cage), the relative rates (specific mass loss rate/Kapton specific mass loss rate) for each set of asher conditions are shown. In Table 7, the rates relative to the 2-Torr, 100-W, no-Faraday-cage condition for each material are shown (specific mass loss rate/specific mass loss rate at 2 Torr, 100 W). Comparison of Tables 5, 6, and 1 shows that use of the Faraday cage gives the best agreement with the flight results; but even so, the agreement is qualitative at best. Without the Faraday cage, only the 2-Torr, 100-W condition gave reasonable agreement with the flight data. Inspection of Table 7 shows that Kapton, polyethylene, and single-crystal graphite show similar relative changes in rate with asher conditions but that FEP Teflon does not, suggesting that FEP Teflon is reacting by a different mechanism. The reactivity of FEP Teflon is greatest at high RF power and low total pressure. Qualitative measurements of the VUV flux at the sample position made with the Watanabe phosphor[61] showed that high Teflon reactivity correlates with high VUV flux at the sample, with or without the Faraday cage.

Results: Flowing Afterglow

The specific reaction rates obtained in the flowing afterglow were substantially lower than those obtained in the asher. The average Kapton specific mass loss rate for all of the afterglow measurements (Table 8) is 3.66 × 10^{-4} mg cm^{-2} min^{-1}. The *Re* of each material is plotted against atom flux in Figs. 3–6. In each figure, the atom flux was varied by changing either the total pressure or water vapor content of the working gas. In Table 8, the materials *Re*, averaged over the range of atom fluxes studied for each working-gas composition, are compared. Inspection of the data in Figs. 5–8 and Table 8 shows that the *Re* of Tedlar and polyethylene vary substantially with atom flux (usually decreasing with increasing atom flux) while the *Re* of Kapton and Mylar are nearly constant. The effects of water vapor and working-gas composition are most easily seen in Table 8. In both 10% O_2 in argon and in O_2, water vapor has little effect on the average *Re* of Tedlar and polyethylene but increases the *Re* of Kapton and Mylar significantly. Changing the working gas from 10% O_2 in argon to O_2 results in lower *Re* for all of the materials, with or without water vapor. In Table 9, the relative rates (specific mass loss rate/Kapton specific mass loss rate) are shown for the various afterglow operating conditions. Reaction efficiency depends on environment even in the relatively benign and well-characterized afterglow, suggesting that processes other than or in addition to oxygen atom attack are involved in the mass loss reaction.

Arrhenius activation energies were determined in the flowing afterglow apparatus. Control experiments showed little disturbance in the atomic oxygen flux at the polymer surface as a result of operating the sample heaters. The results are summarized and compared with literature values in Table 10.

Table 6 Mass loss rates relative to Kapton (plasma asher/Faraday cage)

Pressure, Torr	RF, W	Specific mass loss rate/Kapton rate Kapton	Polyethylene	FEP Teflon	HOPG graphite
2.0	100	1.0	1.8	0.03	——
1.0	100	1.0	——	0.08	——
0.1	100	1.0	——	0.40	——

Table 7 Mass loss rates relative to 2-Torr, 100-W condition, no Faraday cage

Pressure, Torr	RF, W	Mass loss rate/2-Torr, 100-W rate Kapton	Polyethylene	FEP Teflon	HOPG graphite
2	100	1.0	1.0	1.0	1.0
2	50	0.04	0.1	0.7	——
0.4	50	0.5	0.6	1.8	——
0.1	100	0.4	0.7	4.2	0.4
0.1	10	0.08	0.08	1.0	——

Table 8 Average thermal atom reaction efficiencies,[a] *Re*

	Average reaction efficiency (×10^{27} cm^3/atom) Ar/O_2	Ar/O_2, H_2O	O_2	O_2, H_2O
Atom flux range[b]	0.31 ×10^{19}	0.3–1 ×10^{19}	0.3–1 ×10^{19}	1–3 ×10^{19}
Material				
Kapton	0.18±0.05	0.54±0.2	0.12±0.06	0.4±0.2
Mylar	0.27±0.09	0.66±0.2	0.1 ±0.05	0.3±0.08
Polyethylene	4.0±2.1	4.2 ±2.0	0.9 ±0.5	2.4±0.2
Tedlar	3.5±0.9	3.2 ±1.2	0.9 ±0.2	1.7±0.4

[a]The reaction efficiency data shown in Figs. 3–6 are averaged over the range of atom fluxes obtained for each working gas composition. Larger standard deviations indicate greater dependence of *Re* on atom flux.
[b]Atom flux in atoms cm^{-2} s^{-1}.

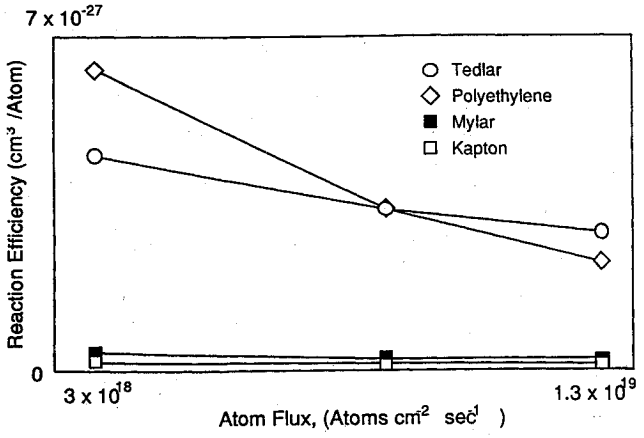

Fig. 3 Reaction efficiency vs atom flux at the sample surface. Atom flux changed by variation of total pressure (Ar/O_2, 90/10, no H_2O vapor).

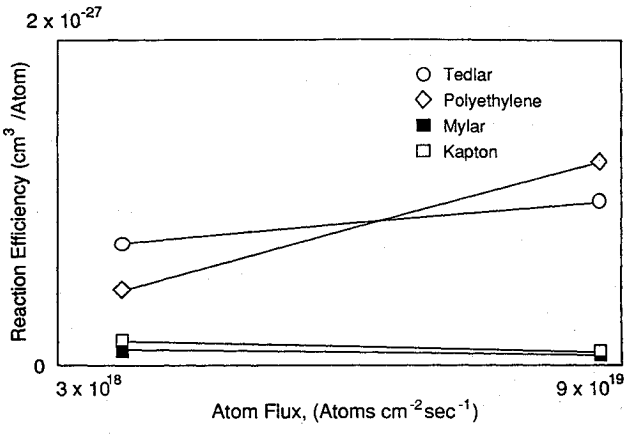

Fig. 5 Reaction efficiency vs atom flux at the sample surface. Atom flux adjusted by variation of total pressure (pure O_2, no H_2O vapor).

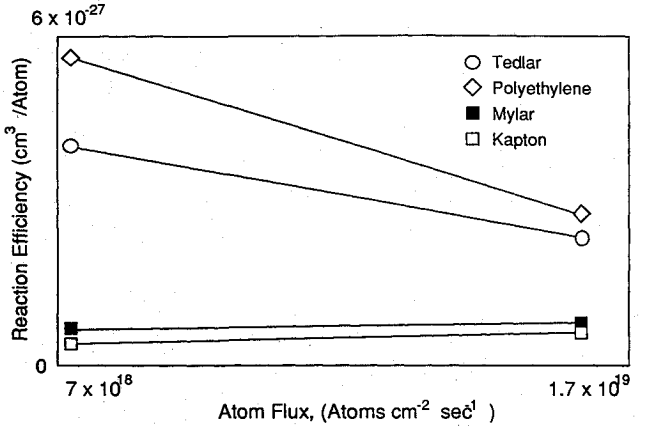

Fig. 4 Mass loss rate vs atom flux at the sample surface. Atom flux varied by variation of H_2O partial pressure at constant pressure (Ar/O_2, 90/10, P = 2 Torr).

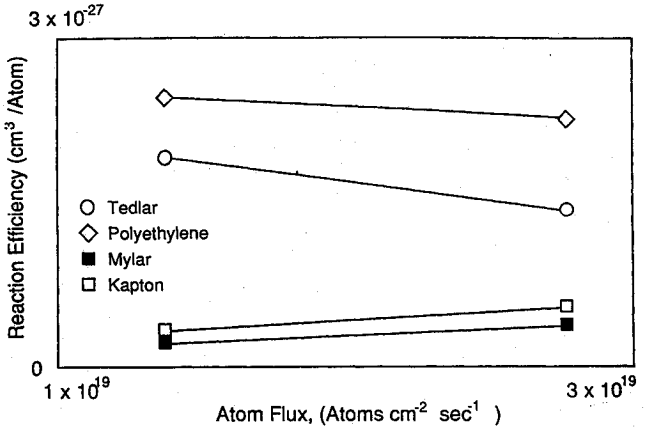

Fig. 6 Reaction efficiency vs atom flux at the sample surface. Atom flux changed by variation of H_2O partial pressure at constant total pressure (pure O_2, P = 2.00 Torr).

Discussion of Results: Plasma Asher

Inspection of Tables 3–7 shows that both the specific mass loss rate and the relative rates of the materials examined vary substantially with asher operating conditions when sample configuration and operating gas are held constant. Without the Faraday cage, only one operating condition produced relative rate data in approximate agreement with flight or high-velocity atom beam data. The changes in relative rates with operating conditions were reduced but not eliminated by enclosing the sample materials in a Faraday cage structure that prevents direct contact between the sample and the plasma. Use of the Faraday cage resulted in significant reductions in specific mass loss rates for all of the materials studied but the effect was most dramatic for FEP Teflon. The results suggest that plasma-asher operating conditions should be selected carefully using a response surface study; i.e., several materials should be tested under a range of asher operating conditions with sample configuration and working-gas type held constant. Those operating conditions producing relative rates in reasonable agreement with space flight and high-velocity beam data should be used in materials screening studies.

The high reactivity of FEP Teflon produced under some conditions shows that misleading data can be produced if plasma ashers are used for materials testing without proper selection of operating conditions. The correlation between Teflon reactivity and VUV-induced fluorescence from the Watanabe phosphor, as well as the overall response surface data, suggests a photochemical reaction mechanism involving VUV radiation. A synergism between VUV radiation and atomic oxygen in the reactivity of FEP Teflon in both flowing afterglow and high-velocity atom beam environments has recently been demonstrated.[27] Even so, other factors such as ions, electrons, and excited-state neutrals cannot be discounted completely in explaining the asher reactivity of FEP Teflon.

The asher conditions producing the best qualitative agreement with flight data produced very good agreement with the flowing afterglow data. Relative rates produced using the Faraday cage or the 2-Torr, 100-W condition were similar to those observed in the afterglow, as can be seen by comparing the data in Tables 5, 6, and 9. Significantly, the *Re* of FEP Teflon in the afterglow (no VUV, no ions, no excited states) is very close to zero.

Discussion of Results: Flowing Afterglow

The *Re* (cm^3/atom) of materials with oxygen atoms at thermal energies has been the subject of considerable uncertainty and speculation, although the bulk of the evidence suggests that thermal atoms are much less reactive than hyperthermal atoms.[59,62,63] The data shown in Figs. 3–6 indicate *Re* values that are 10^{-3} to 10^{-4} those observed in flight (5 eV) or in the hyperthermal (3 eV) beam at LANL. The thermal atom *Re* values reported here do agree in magnitude with those reported by other workers[59,62,63] using thermal energy beam systems where little or no reaction could be detected.

The decrease in *Re* for all materials when the working gas is changed from 10% O_2 in argon to O_2 suggests that high surface fluxes of O_2 somehow slow down the net mass loss reac-

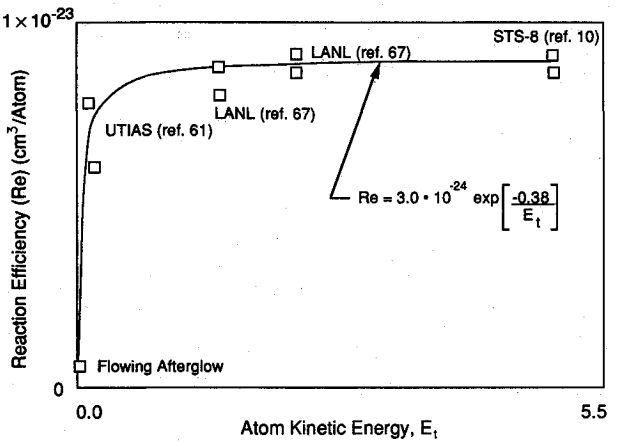

Fig. 7a Reaction efficiency of Kapton as a function of oxygen atom kinetic energy E_t.

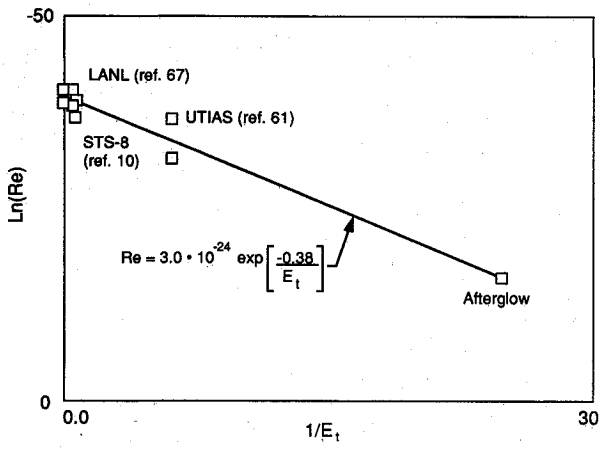

Fig. 7b Reaction efficiency of Kapton as a function of oxygen atom kinetic energy E_t.

tion, although we can only speculate about the mechanism at this time. Water vapor also plays a role in determining *Re*, a role which seems to depend on the chemical structure of the polymer. Water vapor causes an increase in the *Re* of Kapton and Mylar, polymers with a high aromatic hydrocarbon content, but has little effect on polyethylene and Tedlar, the saturated hydrocarbon polymers.

Chemistry of Oxygen Atom Attack on Polymers

The relative reactivities of Kapton, polyethylene, Tedlar, and Mylar lie within a few percent of each other in LEO and in the LANL beam, and range over an order of magnitude in this and other thermal atom systems.[65,66] If the R_E (Table 8) of Kapton, Mylar, Tedlar, and polyethylene are plotted against the atomic fraction of aliphatic hydrogen (*RH* fraction) in the polymer repeat unit, we obtain Fig. 8. The correlation coefficient for *Re* and *RH* fraction is 0.97, indicating a strong relationship between chemical structure and reactivity in the afterglow. Similar correlations can be obtained with the asher 2-Torr, 100-W or Faraday-cage data. Relationships between chemical structure and reactivity have also been reported for the asher environment in connection with photoresist stripping [30] and in other flowing afterglows and plasma ashers.[64,65] Table 1 shows no such relationship between *Re* and chemical structure.

In the gas phase, hydrogen atom abstraction is the first step in the reaction of saturated hydrocarbons and halogenated hydrocarbons with atomic oxygen.[49] In contrast, aromatic

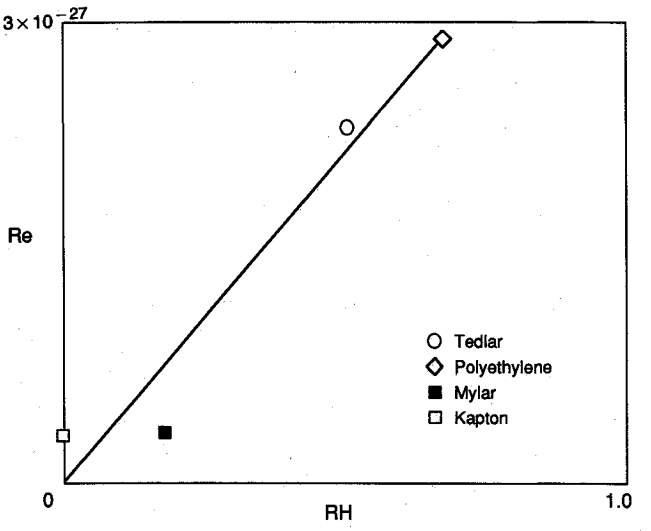

Fig. 8 Reaction efficiency, *Re*, is plotted against the aliphatic hydrogen fraction *RH* in the polymer repeat unit. *RH* is the number of aliphatic hydrogen/total number of atoms. The correlation coefficient for *RH* and *Re* is 0.97; the correlation coefficient for *RH* and log (*Re*) is 0.96; the regression line is $Re = 0.041 + 4.29RH$.

and unsaturated hydrocarbons react by formation of a triplet biradical intermediate that can either decompose directly or rearrange to form an oxygen insertion product[66,67] (e.g., phenol from benzene) with complete reaction to CO, CO_2, and H_2O occurring only after opening of the aromatic ring or destruction of the double bond. The relatively low reaction efficiency of polymers having high aromatic (this work and Refs. 30, 64, 65, 68) or olefinic[68] content is probably related to the formation of triplet biradical intermediates that can crosslink or engage in other side reactions. It is likely (although highly speculative) that mass loss processes cannot begin until the aromatic or olefinic content of the polymer surface is reduced or eliminated and hydrogen abstraction can proceed, leading to the formation of CO, CO_2, and H_2O, the immediate gas-phase reaction products reported for both thermal and hypervelocity atoms.[68,70]

Figure 8 shows how the *Re* of Kapton changes with atom kinetic energy between 0.04 and 5 eV. Despite the range of data sources, the fit to a simple Arrhenius-type function in which atom translational energy replaces kT in the exponential is apparent. The activation energy for the process is 0.38 eV. The activation energy for the gas-phase process

$$R\text{-}H + O \rightarrow R\text{-} + OH$$

Table 9 Flowing afterglow relative rates (*Re*/Kapton *Re*)

Material	Ar/O_2	$Ar/O_2, H_2O$	O_2	O_2, H_2O
Kapton	1	1	1	1
Mylar	1.5	1.2	0.8	0.8
Polyethylene	22	0.8	7.5	6.0
Tedlar	19	5.9	7.5	4.2

Table 10 Sample temperature activation energies

	Activation energies, eV				
Source	JSC afterglow	Boeing[68] afterglow	MSFC[69] asher	STS-8[8,15]	LANL[70]
Atom energy	0.04	0.04	0.04-0.1	5	1.5
Kapton	0.21	0.29	0.13	0.0	0.04
HOPG graphite	0.04	——	——	0.05	——

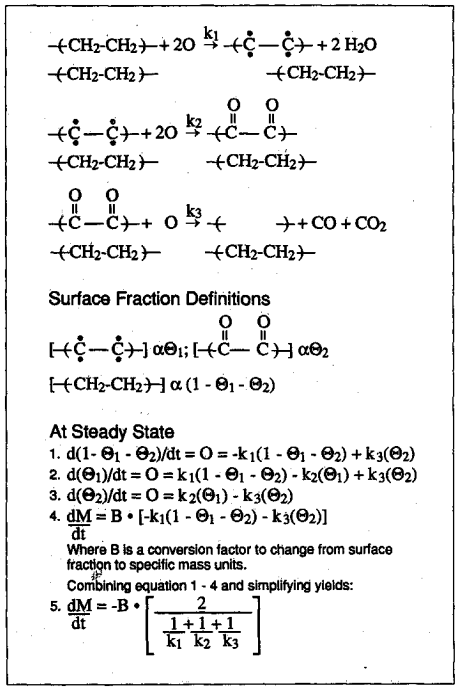

Fig. 9 Speculative kinetic model of the atomic oxygen induced mass loss process on polyethylene.

is between 0.1 and 0.4 eV for the saturated hydrocarbons, alkylamines, and benzene with an average value of 0.24 ± 0.07 eV.[71] The activation energy for oxygen atom insertion in olefins and aromatics is about 0.1 eV.[66,67]

Measurements of the sample temperature dependence of the *Re* (see Table 10) show a change in the character of the rate-limiting step of the mass loss reaction as atom translational energy increases. Activation energies measured in a variety of thermal atom systems (where atom kinetic energy never exceeds 0.06 eV) range from 0.13 to 0.29 eV for Kapton.[72,73] Activation energies measured in the high-energy beam at LANL and in flight range from 0.0 to 0.06 eV for Kapton.[7,74] In contrast, the activation energy for carbon appears to be independent of atom kinetic energy and in reasonable agreement with the values reported by Park.[75]

Many of the observations presented above can be explained with a simple, although highly speculative, phenomenological model describing the kinetics of mass loss when polyethylene is attacked by atomic oxygen. The essentials of the model are shown in Fig. 9. Mass loss occurs sequentially; first hydrogen atoms are removed and some of the resulting radical sites are oxygenated. Mass loss continues via oxygen attack at oxygenated radical sites. The key idea here is that the hydrogen abstraction rate k_1 has a strong dependence on atom kinetic energy (at constant surface temperature) and also varies substantially with the type and quantity of C-H bonds in the material. The four reaction rates depend on atom kinetic energy (and sample surface temperature that is not treated explicitly here), but the hydrogen abstraction rate k_1 is limiting at thermal energies as first proposed by Arnold et al.[62] The model can be easily elaborated or modified to test different reaction mechanisms with different surface intermediates and gas-phase products.

Equation (5) in Fig. 9 shows that at high atom kinetic energies the mass loss rate will be determined by k_2 and k_3. If these constants are similar, all hydrocarbon materials will have similar mass loss rates at high atom energies as shown in Table 1 (polymers containing silicone groups form an inert surface oxide layer that prevents or slows further attack). The model predicts that surfaces exposed to atomic oxygen become oxygen enriched as observed.[42] Finally, the model predicts that substituting deuterium for hydrogen in polyethylene should result in a substantial kinetic isotope shift (i.e., replacing hydrogen with deuterium results in a significant increase in activation energy giving much lower reaction rates)[76] in thermal atom *Re*, but little or no shift in high-energy atom *Re*. Preliminary results on perdeuteropolyethylene obtained in the afterglow system described in this paper show an *Re* on the order of 2.0 times lower than the polyethylene *Re* as expected. In contrast, polyethylene (2.9×10^{-25} cm^3/atom) and perdeuteropolyethylene (2.2×10^{-25} cm^3/atom) show nearly the same *Re* in the LANL high-energy atom beam with a nominal beam energy of 0.8 eV.

Summary and Conclusions

The chemistry and physics of the LEO environment are radically different from those of thermal atom test environments. As a result, materials reactivities and *Re* values are different in the two environments. The *Re* of the materials studied in this work show a strong dependence on atom translational energy. In addition, the dependence of reactivity on sample temperature is different for thermal and hyperthermal atoms, indicating a change in the character of the rate-limiting step as atom translational energy increases. Finally, even the relative reactivities of the various materials are different in the thermal atom and LEO environments. Relative reactivities in thermal atom environments change rapidly with changing operating conditions (even in the relatively benign flowing afterglow) showing that extraneous environmental factors in these systems have a real, observable effect on materials-reactivity measurements, a result that can help explain much of the published data in this field.[81-87] Nishikawa et al.[81] have reported that Teflon and Kapton appear to react by different mechanisms in a capacitively coupled planar plasma-asher system. Operating conditions suitable for materials screening were established by the same type of response surface study reported here.[81]

The available data show that the common practice of reporting "equivalent on orbit oxygen fluence" based on the mass loss rate of Kapton has no basis in physical fact and can be dangerously misleading. Thermal atom systems can serve as credible materials screening tools only if operating parameters are set to provide relative reactivities comparable to those obtained in flight (or in calibrated high-velocity atom beam systems) for a selected materials set, which should contain, as a minimum, Kapton, polyethylene, and FEP Teflon.

The data collected for this review provide insights into the nature of the atomic oxygen reaction with polymer surfaces. At constant sample temperature, the dependence of *Re* on atom translational energy gives an Arrhenius activation energy of 0.38 eV for Kapton, a value comparable to 0.24 eV, the activation energy for the abstraction of hydrogen from saturated hydrocarbons by thermal oxygen atoms in the gas phase, but much higher than 0.1 eV, the activation energy for oxygen atom insertion in olefins and aromatic compounds. We speculate that the aromatic character of Kapton must be reduced or eliminated by oxygen atom insertion before mass loss processes can begin. The sample temperature dependence of the *Re* gives different Arrhenius activation energies with thermal and hyperthermal atoms. A change in the character of the rate-limiting step is indicated as atom translational energy increases from 0.04 to 5 eV.

A simple kinetic model of the reaction of atomic oxygen with polyethylene has been developed. The model predicts the qualitative behavior described in the preceding paragraph. Hydrogen atom abstraction is postulated as the rate-limiting step at thermal atom energies. Oxygen atom translational energy is assumed to be available for overcoming activation barriers, i.e., hydrogen atom abstraction is a direct process. As oxygen atom translational energy increases, other steps in the mass loss process become rate limiting. The model implies that

a substantial kinetic isotope shift should be observed at thermal, but not hyperthermal, atom energies when deuterium replaces hydrogen in the polymer structure. The predicted kinetic isotope shifts have been observed, at least approximately. More work is needed to establish the reaction mechanisms which produce CO and CO_2 as major direct gas-phase products[69,70] in the attack of oxygen atoms on polymer surfaces containing C-H bonds. The model presented can be easily adapted to accommodate a variety of polymer types, reaction mechanisms, and reaction products and should prove useful in improving our understanding of atomic oxygen-materials interactions.

References

[1]Chamberlain, J. W., *Theory of Planetary Atmospheres*, Academic, New York, 1978, p. 305.

[2]Hedin, A. E., Reber, C. A., Newton, G. P., Spencer, N. W., Brinton, H. C., and Mazer, H. G., "A Global Thermospheric Model Based on Mass Spectrometer and Incoherent Scatter Data MSIS 2 Composition," *Journal of Geophysical Research*, Vol. 88, No. A12, 1983, pp. 10,170–10,178.

[3]Leger, L. J., "Oxygen Atom Reactions with Shuttle Materials at Orbital Altitudes," NASA TM-58246, May 1982.

[4]Visentine, J. T., Leger, L. J., Kuminecz, J. F., and Spiker, I. K., "STS-8 Atomic Oxygen Effects Experiment," AIAA Paper 85-0415, Jan. 1985.

[5]Whitaker, A. F., Little, S. A., Harwell, R. J., Griner, D. B., DeHaye, R. F., and Fromhold, A. T., "Orbital Atomic Oxygen Effects on Thermal Control and Optical Materials: STS-8 Results," AIAA Paper 85-0416, Jan. 1985.

[6]Slemp, W. S., Santos-Mason, B., Sykes, G. F., and Witte, W. G., "Effects of STS-8 Atomic Oxygen Exposure on Composites, Polymeric Films, and Coatings," AIAA Paper 85-0418, Jan. 1985.

[7]Gregory, J. C., and Peters, P. N., "Measurement of Reaction Rates and Activation Energies of 5-eV Oxygen Atoms with Graphite and Other Solid Surfaces," AIAA Paper 85-0417, Jan. 1985.

[8]Peters, P. N., Gregory, J. C., and Swann, J. T., "Effects on Optical Systems from Interactions with Oxygen Atoms in Low Earth Orbits," *Applied Optics*, Vol. 25, No. 8, April 1986, pp. 1290–1298.

[9]Smith, K. A., "Evaluation of Oxygen Interaction with Materials (EOIM): STS-8 Atomic Oxygen Effects," AIAA Paper 85-7021, Jan. 1985.

[10]Park, J. J., Gull, T. R., Herzig, H., and Toft, A. R., "Effects of Atomic Oxygen on Paint and Optical Coatings," AIAA Paper 83-2634, Oct.–Nov. 1983.

[11]Stuckey, W. K., "Effects on Optical and Metallic Surfaces," AIAA Paper 83-2635, Oct.–Nov. 1983.

[12]Slemp, W. S., "Effects of Atomic Oxygen on Composites and Thermal Control Coatings," AIAA Paper 83-2633, Oct.–Nov. 1983.

[13]Whitaker, A. F., "LEO Atomic Effects on Spacecraft Materials," AIAA Paper 83-2632, Oct.–Nov. 1983.

[14]Leger, L. J., Spiker, I. K., Kuminecz, T. J., Ballentine, T. J., and Visentine, J. T., "STS-5 LEO Effects Experiment—Background Description and Thin Film Results," AIAA Paper 83-2631, Oct.–Nov. 1983.

[15]Meshishnek, M. J., Stuckey, W. K., Evangelides, J. S., Feldman, L. A., Peterson, R. V., Arnold, G. A., and Peplinski, D. R., "Effects on Advanced Materials: Results of STS-8 EOIM Experiment," Aerospace Corp., Los Angeles, CA, Rept. SD-TR-87-34, July 1987.

[16]Liang, R., and Gupta, A., "Mechanistic Studies of Kapton Degradation in Shuttle Environments," AIAA Paper 83-2656, Oct.–Nov. 1983.

[17]Whitaker, A. F., Burka, J. A., Coston, J. E., Dalins, I., Little, S. A., and DeHaye, R. F., "Protective Coatings for Atomic Oxygen Susceptible Spacecraft Materials—STS-41G Results," AIAA Paper 85-7017, Nov. 1985.

[18]Zincik, D. G., and Maag, C. R., "Results of Apparent Atomic Oxygen Reactions with Spacecraft Materials," *Journal of Spacecraft and Rockets*, Vol. 25, March–April 1988, pp. 162–167.

[19]Fromhold, A. T., Daneshvar, K., Whitaker, A. F., and Little, S. A., "Reaction of Metals in Low Earth Orbit During Space Shuttle Flight 41-G," AIAA Paper 85-7018, Nov. 1985.

[20]Ousley, G. W. (ed.), *Proceedings of the SMRM Degradation Study Workshop*, May 9–10, 1985, Goddard Space Flight Center, Greenbelt, MD, 408-SMRM-0001, pp. 211–343.

[21]Gregory, J. C., and Peters, P. N., "A Measurement of the Angular Distribution of 5-eV Atomic Oxygen Scattered Off a Solid Surface in Earth Orbit," *Rarefied Gas Dynamics*, Vol. 15, 1987.

[22]Peters, P. N., Sisk, R. C., and Gregory, J. C., "Velocity Distributions of Oxygen Atoms Incident on Spacecraft Materials," *Journal of Spacecraft and Rockets*, Vol. 25, Jan.–Feb. 1988, pp. 53–58.

[23]Leger, L. J., Santos-Mason, B., Visentine, J., and Kuminecz, J., "Review of LEO Flight Experiments," *Proceedings of the NASA Workshop on Atomic Oxygen Effects*, Nov. 1986, NASA Jet Propulsion Lab., Pasadena, CA, Pub. 87-14, June 1987, pp. 1–10.

[24]Leger, L. J., Visentine, J., and Santos-Mason, B., "Selected Materials Issues Associated with Space Station," *SAMPE Quarterly*, Vol. 18, No. 2, Jan. 1987, pp. 48–54.

[25]Leger, L. J., and Visentine, J. T., "A Consideration of Atomic Oxygen Interactions with Space Station," *Journal of Spacecraft and Rockets*, Vol. 23, No. 5, Sept.–Oct. 1986, pp. 505–511.

[26]Durcanin, J. T., Chalmers, D. R., and Visentine, J. T., "The Definition of the Low Earth Orbital Environment and Its Effect of Thermal Control Materials," AIAA Paper 87-159, June 1987.

[27]Kootnz, S. L., Leger, L. J., Albyn, K. A., and Cross, J., "Ultra-Violet Radiation/Atomic Oxygen Synergism in Materials Reactivity," *Journal of Spacecraft and Rockets*, Vol. 27, No. 5, 1990, pp. 346–348.

[28]Boening, H. V., *Plasma Science and Technology*, Cornell University Press, Ithaca, NY, 1982, Chap. 1.

[29]Kaufman, F., *Progress in Reaction Kinetics*, Vol. 1, Pergamon Press, London, 1961, pp. 1–39.

[30]Hartney, M. A., Hess, D. W., and Soane, D. S., "Oxygen Plasma Etching for Resist Stripping and Multilayer Lithography," *Journal of Vacuum Science and Technology B*, Vol. 7, Jan.–Feb. 1989, p. 1.

[31]Nasser, E., *Fundamentals of Gaseous Ionization and Plasma Electronics*, Wiley-Interscience, 1971.

[32]Lewellyn-Jones, F., *The Glow Discharge*, Methuen, London, 1966.

[33]Suzuki, K., Sadayuki, O., and Kanomata, I., "The Roles of Ions and Neutral Active Species in Microwave Plasma Ashing," *Journal of the Electrochemical Society*, Vol. 126, Pt. I, No. 1–6, Jan.–June 1979, pp. 1024–1028.

[34]Jacob, A., United States Patent 4,362,632, Dec. 7, 1982.

[35]Visser, R. J., and de Vries, C. A. M., *Proceedings of the 8th International Symposium on Plasma Chemistry*, Pergamon, England, 1987, p. 1029.

[36]Eggito, F. D., Emmi, F., Horwath, R. S., and Vukanovis, V., *Journal of Vacuum Science Technology B*, Vol. 3, No. 4, 1985, p. 893.

[37]Evans, J. F., Newman, J. G., and Gibson, J. H., *Surface and Colloid Science in Computer Technology*, edited by K. L. Mittal, Plenum Press, New York, 1986, p. 299.

[38]Choe, D., Knapp, C., and Jacob, A., "Production RIE-II: Selective Aluminum Alloy Etching," *Solid State Technology*, March 1985, pp. 165–171.

[39]Choe, D., Knapp, C., and Jacob, A., "Production RIE-II: Selective Dielectric Etching," *Solid State Technology*, April 1984, pp. 177–183.

[40]Tolliver, D. L., "Plasma Processing in Microelectronics—Past, Present, and Future," *Solid State Technology*, Nov. 1980, pp. 99–105.

[41]Finlayson-Pitts, B. J., and Pitts, J. N., Jr., *Atmospheric Chemistry: Fundamentals and Experimental Techniques*, Wiley, New York, 1986, Chap. 7.

[42]Golub, M. A., and Wydeven, T., "ESCA Study of Kapton Exposed to Atomic Oxygen in Low Earth Orbit or Downstream from a Radio Frequency Oxygen Plasma," *Polymer Communication*, Vol. 25, Oct. 1988, pp. 285–288.

[43]"Space Station Natural Environment Definition for Design," Johnson Space Center, Houston, TX, JSC 30425, Jan. 1987.

[44]Zaidel, A. N., and Shreider, E. Y., *Vacuum Ultraviolet Spectroscopy*, Ann Arbor-Humphrey Science Publishers, Michigan, 1970, Chaps. 1, 4.

[45]Tanaka, I., and Lossing, F. P., "Photoionization as a Source of Ions for Mass Spectroscopy," *Journal of Chemical Physics*, Vol. 25, No. 5, Nov. 1956, pp. 1031–1034.

[46]Clyne, M. A. A., and Nip, W. S., "Generation and Measurement of Atom and Radical Concentrations in Flow Systems," *Reactive Intermediates in the Gas Phase*, edited by D. W. Stezer, Academic Press, New York, 1979, pp. 1–57.

[47]Krogelb, S., and Stranberg, W. P., "Use of Paramagnetic-Resonance Techniques in the Study of Atomic Oxygen Recombination," *Journal of Chemical Physics*, Vol. 31, No. 5, Nov. 1959, pp. 1196–1210.

[48]Finlayson-Pitts, B. J., and Pitts, J. N., Jr., *Atmospheric Chemistry: Fundamentals and Experimental Techniques*, Wiley, New York,

1986, Chap. 4.

[49]Herron, J. T., and Huie, R. E., "Rate Constants for the Reactions of Atomic Oxygen (O^3P) with Organic Compounds in the Gas Phase," *Journal of Chemical Physics Reference Data*, Vol. 2, No. 3, 1973, pp. 467–517.

[50]Paraszczak, J., Hatzakis, M., Babich, E., Shaw, J., and Arthur, E., "Plasma Etching of Polymers for Multilayer Lithography, *Microcircuit Engineering*, Academic Press, New York, 1985.

[51]DeJaegere, S., Willems, M., and Vinckler, C., "Interactions Between Afterglow Products of Microwave-Induced Plasmas and Solids," *Journal of Physical Chemistry*, Vol. 86, 1982, pp. 3569–3577.

[52]Dzioba S., Este, G., and Naguib, H. M., "Decapsulation of Photoresist Stripping in Oxygen Microwave Plasma," *Journal of the Electrochemical Society*, Vol. 86, 1982, pp. 3569–3577.

[53]Harteck, P., and Reeves, R. R., Jr., "Formation and Reactions of the Excited $O_2(^3\Sigma_u^+)$ Molecules," *Discussions of the Faraday Society*, Vol. 37, 1964, p. 82.

[54]Halstead, J. A., and Triggs, N., "Creation of Electronically Excited States by Heterogeneous Catalysis," *Gas-Phase Chemiluminescence and Chemi-Ionization*, edited by A. Fontijn, Elsevier, London, 1985, pp. 307–326.

[55]Chu, A., Reeves, R. R., and Halstead, J. A., "Surface-Catalyzed Formation of Electronically Excited Nitrogen Dioxide and Oxygen," *Journal of Physical Chemistry*, Vol. 90, No. 3, 1986, pp. 466–467.

[56]Eggers, D. F., Jr., Gregory, N. W., Halsey, G. D., Jr., and Rabinovitch, B. S., *Physical Chemistry*, Wiley, New York, 1964, Chap. 6.

[57]Dushman, S., and Lafferty, J. M., *Scientific Foundations of Vacuum Technique*, Wiley, New York, 1962, Chap. 1.

[58]Brown, R. L., "Tubular Flow Reactors with First-Order Kinetics," *Journal of Research of the National Bureau of Standards*, Vol. 83, No. 1, pp. 1–8.

[59]Koontz, S. L., and Nordine, P., *Materials Degradation in LEO*, edited by V. Srinivasan and B. A. Banks, TMS Minerals, Metals, and Materials, Warrendale, PA, 1990, pp. 189–206.

[60]Koontz, S. L., Albyn, K., and Leger, L., "Materials Selection for Long Life in LEO: A Critical Evaluation of Atomic Oxygen Testing with Thermal Atom Systems, *Journal of the IES*, March–April 1990, pp. 50–59.

[61]Watanabe, K., *Physical Review*, Vol. 83, 1951, p. 785.

[62]Arnold, G. S., Peplinski, D. R., and Cascarano, F. M., "Translational Energy Dependence of the Reaction of Atomic Oxygen with Polyimide Films," *Journal of Spacecraft and Rockets*, Vol. 24, No. 5, 1987, pp. 454–458.

[63]Zimcik, D. G., and Maag, C. R., "The Results of Apparent Atomic Oxygen Reactions with Spacecraft Materials During Shuttle Flight STS-41G," *Journal of Spacecraft and Rockets*, Vol. 25, No. 2, 1988, pp. 162–167.

[64]Hansen, R. H., Pascale, J. V., DeBenedictis, T., and Rentzepis, P. M., "Effects of Atomic Oxygen on Polymers," *Journal of Polymer Science*, Pt. A, Vol. 3, June 1965, pp. 2005–2214.

[65]Golub, M. A., and Wydeven, T., "Reactions of Atomic Oxygen (O^3P) with Various Polymer Films," *Polymer Degradation and Stability*, Vol. 22, 1988, pp. 325–338.

[66]Sibener, S. J., Buss, R. J., Piergiorgio, C., Hirooka, T., and Lee, Y. T., "A Crossed Molecular Beams Investigation of the Reactions of $O^3P + C_6H_6, C_6D^6$," *Journal of Chemical Physics*, Vol. 72, April 1980, pp. 4341–4349.

[67]Cvetanovic, R. J., "Addition of Atoms to Olefins in the Gas Phase," *Advances in Photochemistry*, Vol. 1, 1063, pp. 115–182.

[68]Golub, M. A., Lerner, N. R., and Wydeven, T., "Reactions of Atomic Oxygen (O^3P) with Polybutadienes and Related Polymers," *Chemical Reactions on Polymers*, edited by J. L. Benham and J. F. Kinstle, ACS Symposium Series No. 364, American Chemical Society, Washington, DC, 1988, Chap. 25.

[69]Chou, N. J., Parazczask, E. B., Chaug, Y. S., and Goldblat, R., "Mechanisms of Microwave Plasma Etching of Polyimides in O_2 and CF_4 Gas Mixtures," *Microelectron Eng.*, Vol. 5, 1986, pp. 375–386.

[70]Cross, J. B., Koontz, S. L., and Gregory, J. C., "Laboratory Investigations Involving High-Velocity Oxygen Atoms," *Proceedings of the Advanced Aerospace Materials Symposium*, 119th TMS Annual Meeting and Exhibit, TMS, Warrendale, PA, Feb. 1990, pp. 1–14.

[71]Kerr, J. A., and Moss, S. J. (eds.) *CRC Handbook of Bimolecular and Thermolecular Gas Phase Reactions*, Vol. 1, CRC Press, Boca Raton, FL, 1981, pp. 66–70.

[72]Pippin, H. G., Torre, L. P., Linton, R. G., and Witaker, A. F., "Materials Resistance to Low-Earth Orbit Environment Effects," *Proceedings of the 34th International SAMPE Symposium and Exhibition*, Vol. 34, SAMPE, Covina, CA, May 1989, pp. 1143–1151.

[73]Personal communication, A. F. Witaker, NASA Marshall Space Flight Center, Huntsville, AL, 1989.

[74]Leger, L. J., Koontz, S. L., Visentine, J. T., and Cross, J. B., "Laboratory Investigations Involving High-Velocity Oxygen Atoms," *Proceedings of the Fourth International Symposium on Spacecraft Materials in Space Environment*, Centre d'etudes et de Recherches de Toulouse, Toulouse, France, Sept. 1988, pp. 393–404.

[75]Park, C., "Effect of Atomic Oxygen on Graphite Ablation," *AIAA Journal*, Vol. 14, Nov. 1976, pp. 1640–1642.

[76]Melander, L., and Sanders, W. H., *Reaction Rates of Isotopic Molecules*, Wiley, New York, 1980, Chaps. 1, 2, 5.

[77]McCargo, M., M. Dammann, R. A., Cummings, R. T., and Carpenter, C., "Laboratory Investigation of the Stability of Organic Coatings for Use in a LEO Environment," *Proceedings of the Third European Symposium on Spacecraft Materials in Space Environment*, Paris, France, European Space Agency, Pub. ESA SP-232, Nov. 1985, pp. 91–97.

[78]Colony, J. A., and Sanford, E. L., "*Mechanisms of Polymer Degradation Using an Oxygen Plasma Generator*," NASA TM-100681, Sept. 1987.

[79]Banks, B. A., Rutledge, S. K., and Brady, J. A., "The NASA Atomic Oxygen Effects Test Program," *Proceedings of the 15th Space Simulation Conference*, NASA CP-3015, 1988, pp. 51–65.

[80]Knopf, P. W., Martin, R. J., Damman, R. E., and McCargo, M.,"Correlation of Laboratory and Flight Data for the Effects of Atomic Oxygen on Polymeric Materials," AIAA Paper 85-1006, June 1985.

[81]Nishikawa, T., Sonoda, K., and Nakanashi, K., "Effects of Atomic Oxygen on Polymers Used as Surface Materials for Spacecraft," *Proceedings of the 21st Symposium on Electrical Insulation Materials*, Scientific Publishing Div., MYU, Tokyo, Japan, 1988, pp. 191–194.

Henry B. Garrett
Associate Editor